01 Jan 2017

Control of Columnar to Equiaxed Transition in Solidification Macrostructure of Austenitic Stainless Steel Castings

Semen Naumovich Lekakh
Missouri University of Science and Technology, lekakhs@mst.edu

Ronald J. O'Malley
Missouri University of Science and Technology, omalleyr@mst.edu

Mark C. Emmendorfer

Brenton Hrebec

Recommended Citation

S. N. Lekakh et al., "Control of Columnar to Equiaxed Transition in Solidification Macrostructure of Austenitic Stainless Steel Castings," *ISIJ International*, vol. 57, no. 5, pp. 824-832, The Iron and Steel Institute of Japan (ISIJ), Jan 2017.
The definitive version is available at https://doi.org/10.2355/isijinternational.ISIJINT-2016-684

ISIJ International, Vol. 57 (2017), No. 5, pp. 824–832

Control of Columnar to Equiaxed Transition in Solidification Macrostructure of Austenitic Stainless Steel Castings

Simon Naumovich LEKAKH,* Ron O'MALLEY, Mark EMMENDORFER and Brenton HREBEC

Missouri University of Science and Technology, Rolla, MO, 65409 USA.

(*Received on November 30, 2016; accepted on January 26, 2017*)

Solidification macrostructure is of great importance for the properties and the quality of castings made from austenitic grade stainless steels (ASS) because there are limited options to change as-cast macrostructure in the solid condition. A typical cast macrostructure of ASS has a fine surface chilled zone followed by an elongated dendrite zone, columnar to equiaxed transition (CET) zone, and centrally located equiaxed crystals. Several castings from ASS were produced to determine the effects of casting geometry, chilling, and grain refinement on CET. The transient thermal field in solidified heavy castings was simulated and used to determine an isotherm velocity (V) and the thermal gradient (G) in mushy zone at 50% solid fraction. The critical value of the parameter G^n/V was determined from the macrostructure of the cylindrical casting. Using this value, the location of CET was predicted in the heavy rectangular casting and this prediction was in agreement with experimental macrostructure. Two methods of controlling casting macrostructure by using a chilled mold to stimulate extensive columnar zone and by using melt grain refinement to produce fine equiaxed crystals were experimentally verified and simulated.

KEY WORDS: solidification; CET; grain refinement; stainless steel.

1. Introduction

1.1. Solidification Structure Control

A typical cast macrostructure of austenitic stainless steel (ASS) alloyed by *Cr*, *Ni*, *Mo* and the other transition metals has a fine surface chilled zone followed by an elongated dendrite zone and centrally located equiaxed crystals. The size and morphology of primary grains are of particular importance for physicochemical and mechanical properties of ASS. The grain size in the columnar and equiaxed zones, their ratio, and a columnar-to-equiaxed transition (CET) are the main parameters which characterize ASS solidification macro-structure. A CET zone in high alloy ASS is considered to be a possible place for element segregation and agglomeration of undesirable structural features (inclusion, micro-porosity *etc.*).

The solidification macrostructure of ASS can be modified in two ways:

(i) A fully columnar grain structure can be promoted. The oriented columnar and single grain cast structures of this type are very effective for high temperature applications, such as for directionally solidified aircraft turbine blades.[1] Chills are often employed in ASS castings produced in sand molds for this purpose and to control shrinkage porosity.

(ii) A fully equiaxed grain structure can be promoted. Grain refining extends the equiaxed zone and can partially or fully suppresses the columnar dendrite zone.[2]

Grain refinement of the cast structure is an important tool for reducing compositional micro-segregation within grains, for decreasing the large scale macro segregation of alloying elements within the entire casting, and for controlling the structure and composition of the grain boundaries. Control of the solidification structure by grain refining does not have casting geometry restrictions. Effective grain refinement requires the enhancement of heterogeneous nucleation during solidification. There are a variety of technical approaches that have been developed for cast structure grain refinement. These approaches are based on different principles which can be classified into two groups. The first group of methods can be referred to as physical methods, which involve the breaking of nuclei from dendrite branches by mechanical or electromagnetic stirring.[3–5] The second group is comprised of so-called, "chemical" methods, which employ special additives to develop active heterogeneous nuclei.[2,6–8]

1.2. Simulation of Solidification Macrostructure in Heavy Castings

In his seminal publication, Hunt[9] established the theory of columnar-to-equiaxed transition (CET). During columnar growth, aligned dendrites grow opposite to the heat flow direction, from the casting wall toward the center of the casting. When the necessary chemical and thermal conditions are developed, equiaxed crystals grow in the melt ahead of the dendrite tips, which stops the dendrites from growing. This will happen when a critical fraction of equiaxed grains is achieved. For the suggested critical fraction of 0.49, the temperature gradient G (°C/mm) at the

* Corresponding author: E-mail: lekakhs@mst.edu
DOI: http://dx.doi.org/10.2355/isijinternational.ISIJINT-2016-684

dendrite tip will be less than:[9]

$$G < 0.617N^{1/3}\left[1-\left(\Delta T_N / \Delta T_C\right)^3\right]\Delta T_C \quad \text{..... (1)}$$

where: N is the heterogeneous nuclei density (mm^{-3}), ΔT_N is supercooling necessary for nucleation, and ΔT_C is constitutional undercooling on the dendrite tip.

Constitutional undercooling ΔT_C is defined by Eqs. (2) and (3):

$$\Delta T_C = \left(VC_0 / A\right)^{1/2} \quad \text{..... (2)}$$

$$A = D/\left[8m\left(k-1\right)\Gamma\right] \quad \text{..... (3)}$$

where: V is the dendrite tip velocity (mm/min), D is the diffusion coefficient of solute element, m is the liquidus slope, k is the partitioning coefficient, and Γ is the Gibbs-Thomson parameter.

It is widely accepted that for technical purity alloys $\Delta T_N/\Delta T_C << 1$ and after arranging Eqs. (1)–(3) the Hunt's criterion for CET will be:

$$G / V^{0.5} < 0.617N^{1/3}\left(C_0 / A\right) \quad \text{..... (4)}$$

The Hunt criterion was established for a 2D solidification case in assumption that a critical fraction of equiaxed grains will arrest the growth of columnar grains (**Fig. 1**(a)). The Hunt's criterion is shown by dashed line on a G-V Hunt map (Fig. 1(b)). The slope of this line depends on nuclei density, alloy composition, an assumption about a critical fraction of equiaxed grains, dendrite growth kinetics, *etc.*, and was verified in many publications using more sophisticated micro-models. A review article[10] summarized recent progress in computational modeling of CET in solidified alloys.

In direct methods, equiaxed solidification was treated simultaneously with columnar.[11,12] Two micro-models for dendritic and equiaxed envelops growth, fully coupled with computational fluid dynamic (CFD) simulated heat extraction from the casting, were used to track the CET.[12] In the model, the equiaxed grains compete with the advancing columnar grains. It was assumed that the CET occurred at 0.49 volume fraction of equiaxed grains. The method provided realistic trends of the effects of alloy composition, surface cooling flux, and pouring superheat on the CET. It was found that the nucleation constant used in simulations needed to be altered to match the experimentally observed position of the CET. The Hunt map was in reasonable agreement with the obtained *G-V* trend of the CET.

Phase-field simulation has been used to simulate micro-modelling of the CET considering solute partitioning, diffusion and constitutional undercooling near the solidification front.[13] While there is reasonable similarity between the simulated Hunt map, micro-modelling provides a better understanding of the microstructural nature of the CET. More complicated meso-scale front-tracking models (FTM) with incorporated Kurz, Giovanola, and Trivedi (KGT) dendrite kinetics and the Scheil solidification path have also been developed to predict CET in castings in the presence of natural thermal convection.[14] Experiments with directional solidification of aluminum alloys supported the importance of natural convection for the blockage of columnar grains. The blockage distance was shortened in the case of horizontal growth versus solidification of the same alloy in vertical direction, while the effect of alloy composition was not determined.[15]

Gandin and Rappaz explored the possibility of coupling finite element heat flow computations with cellular automata (CA) calculations describing the mechanisms of nucleation and growth of dendrite grains.[16] This modelling approach was referred to as cellular automata-finite element (CAFÉ) method. Later, the authors extended a model to non-uniform temperature situations in three-dimensional space[17] and the developed 3D CAFÉ module was incorporated into commercial ProCAST software.[18] The CAFÉ ProCAST module has found wide application in the simulation of directionally solidified turbine blades for *Ni*-based alloys,[1] complicated shape sand castings,[19] and continuously cast billets.[20] The CAFÉ method was also used to optimize grain selector in a spiral to produce a single crystal casting.[21] The CAFÉ model was recently used for complex analysis of the solidification process in ingots from *Fe–Mn–C* TWIP steel, including shrinkage porosity, microsegregation, grain structure, and CET.[22] When comparing two Hunt maps for different TWIP steels, higher alloying results in a widening of the equiaxed zone both by enlarging the constitutional undercooling range and increasing the temperature in front of the liquid/solid interface.

Several coefficients that characterize the Gaussian distribution of nucleation sites need to be verified from experiments. To present alloy properties in the CAFÉ model, thermodynamic simulations are used to estimate liquidus slope and solute partitioning for calculation of two coefficients a_2 and a_3 of dendrite growth velocity (V) as a function of supercooling ΔT:

$$V = a_2\Delta T^2 + a_3\Delta T^3 \quad \text{..... (5)}$$

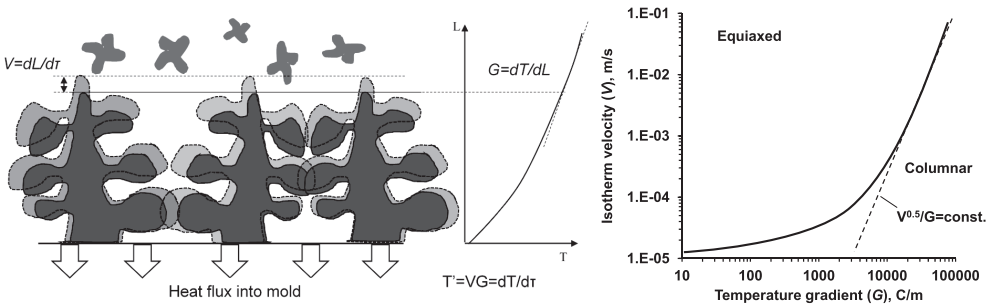

(a) (b)

Fig. 1. Schematics of CET in solidified alloy (a) and a G-V Hunt map (b).

The CET simulation on a macro-scale (>1 mm), considering coupling with microscopic scale (<1 mm) scientific phenomena, is still a challenge.[10] Using macro-scale models with embedded microscopic phenomena requires the assumption of several arbitrary parameters which need to be verified in experiments. A large number of unknown variables make it difficult to tune simulation results because of possible non-linear effects and mutual dependences. On the other hand, a simplified macro-scale model based on Hunt map has a significantly fewer number of unknown parameters but predicts similar *G*-*V* trends to those obtained from the more sophisticated micro-models.

Here it is necessary to mention that the Hunt model can only predict the CET, while micro-models simulate the whole grain structure. Also, the constant G^n/V relationship is only valid in the processing window when the nucleation undercooling is small. This assumption has been confirmed to be reasonable for the analysis of solidification structures in many industrial processes, such as welding, casting, or laser treatment.[23]

The prediction of the CET in industrial castings based on the Hunt map is supported by experiments in many studies.[23–27] The parameter n in Hunt's criterion G^n/V= constant was verified by Kurz, Bezenson, and Gauman[23] and the modified value n = 3.4 was recommended. Prediction of the CET in continuous casting 16% Cr ferritic stainless steel was performed using a macro-simulated G^n/V number and a reasonable agreement with experimental structure was obtained at 0.5 solid fraction for different superheats with and without electromagnetic stirring (EMS). In addition, the effect of nominal superheat was not significant with EMS application.[24] Prediction of the equiaxed crystal ratio in a continuously cast steel slab was performed for ferritic steel using the Hunt model.[25] The G^n/V parameter was simulated at a solid fraction of 0.3. The Hunt model explained the effects of the casting speed, melt superheat, steel composition, EMS and cooling intensity of the position of CET in the slab. A combination of the macro-CFD simulation of the thermal field with the Hunt *G*-*V* map successfully predicted the CET in re-melted ingots from a nickel-based superalloy.[26] CET in inoculated aluminum alloys was investigated using measured cooling curves. These cooling curves were superimposed on simulated Hunt type map.[27] The experimental G and V values were determined from cooling curves at the liquidus temperature while the predicted position of the CET was closer to the base of the ingot than observed experimentally.

In this article, the possibility of tracking CET in heavy section ASS castings using the modified Hunt's criterion $G^{3.4}/V$= constant[23] was explored. A combination of CFD simulations with experimental measurements was used. In the first part of the article, the predicted results were compared to the experimental macrostructure. In the second part, this approach was used to analyze the mechanisms that control the macrostructure.

2. Procedures

2.1. Experimental

To study macrostructure, heavy section castings were produced from high alloy stainless steel (**Table 1**).

Steel was melted in an induction furnace. Two melt treatments were investigated: the first one included *Ca*-treatment ("base") and the second one employed grain refining treatment ("refined"). Heterogeneous nucleation of austenite was facilitated by sequential formation of Al–Mg spinel dispersoids in the melt followed by co-precipitation of TiN on dispersoid surfaces above the liquidus temperature during melt cooling. The details of grain refining treatments are described elsewhere.[2]

A set of the experimental castings included:

Type A: two castings ("base" and "refined" ASS), each 4" (101 mm) in diameter and 8" (203 mm) tall vertical cylinders with top risers 6" (152 mm) in diameter and 4" (101 mm) tall produced in no-bake quartz sand molds. A bottom gating system was used to achieve a uniform initial temperature distribution (**Fig. 2**(a)). Two *S*-type thermocouples in quartz tubes (additionally protected by ceramic stucco) were installed at 4" (101 mm) from the bottom: the first one at 0.5" (12 mm) radius (near the center) and the second one at

Table 1. Compsition of high alloyed austenitic steel, wt.%.

Cr	*Ni*	*Mo*	*Cu*	*Mn*	*Si*	*C*
19.4	18.4	6.5	0.7	0.5	0.6	0.01

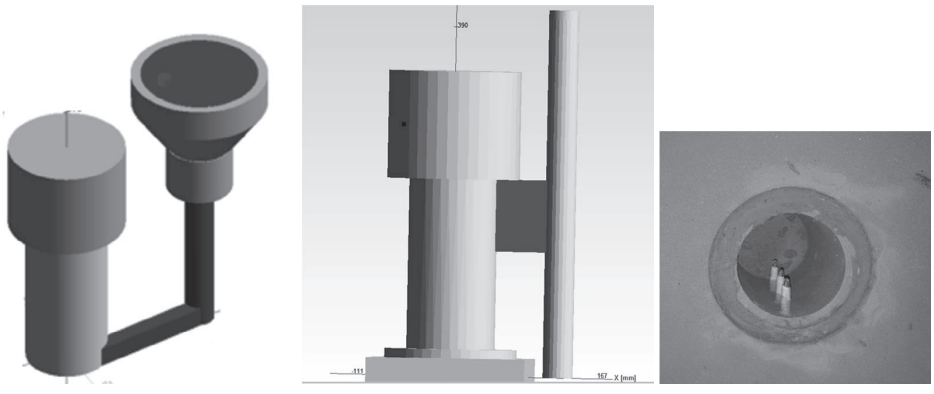

(a) (b) (c)

Fig. 2. Experimental castings: (a) casting "A", (b) casting "C" with bottom chill, and (c) three thermocouples installed in casting "C" (top view).

3" (76 mm) radius (near the wall) (Fig. 2(a));

Type B: one casting ("base" ASS) with a heavy section rectangular block with dimensions: 6" (152 mm) × 15" (381 mm) and 6" (152 mm) tall. No-bake quartz sand molds with a bottom gating system and a cylindrical top riser were used;

Type C: one casting ("base" ASS) with a similar geometry to casting "A" but designed for directional solidification. A copper water-cooled chilling plate was incorporated in the bottom of the mold cavity. The design also included a 5" (127 mm) diameter, 1/4" (6 mm) thick addition to the casting bottom to increase cooling intensity. A low thermal conductivity insulation sleeve with a 4" (101 mm) internal diameter and 0.5" (12 mm) wall thickness surrounded by no-bake sand was used to decrease heat flux in radial direction. A side gating system was used for this casting to avoid additional heating of the chill during mold pouring (Fig. 2(b)). Three *S*-type thermocouples were installed in the cooling direction at 1.5" (38 mm), 3" (76 mm) and 5" (127 mm) from the chill (Fig. 2(c)).

Castings were sectioned along the middle horizontal and vertical planes, milled, ground, and macro-etched using the mixture of ten parts of pure hydrochloric acid and one part of concentrated hydrogen peroxide.

2.2. Simulations

Transient (time dependent) heat transfer between the solidified casting, the mold, and the environment coupled with buoyancy-driven melt convection flow in the mold cavity was simulated using commercial Computational Fluid Dynamic (CFD) FLUENT software. Details of applied governing equations are given in the User Manual[28] and specific simulation details are given in **Table 2**.

Simulations were performed using transient solvers: (i) coupled Energy and Laminar Flow in gravity (Method 1, "flow") or, for sake of simplicity, (ii) only transient Energy solvers assuming immobile melt and temperature dependent atomic heat conductivity in the melt[29] (Method 2, "no flow"), or (iii) applying approximately the 5 times increased coefficient of heat conductivity (K_{aj}) of the melt to compensate increased intensity of heat transfer by melt convection [25] at temperatures above the temperature of dendrite coherency (Method 3, "adjusted *K*").[30]

Two solidification parameters were defined at approximately 50% of solid fraction. The parameters were isotherm velocity (*V*, m/sec) and thermal gradient (*G*, C/m) in the mushy zone. This fraction of solid phase in equiaxed zone was considered to be able to stop impingement of columnar crystals.[9] The calculation procedure included tracking of the position and velocity of two close isotherms (2°C difference). **Figure 3** illustrates two isotherms (1 381°C and 1 383°C) in a vertical central section of the solidified casting "A". The local thermal gradient *G* was defined as the dis-

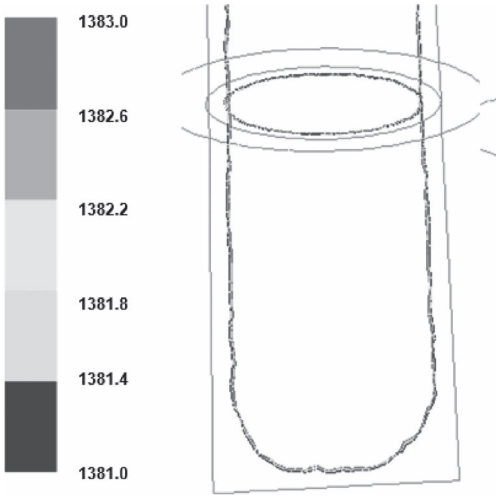

Fig. 3. Two moving isotherms (1 381°C and 1 383°C) from CFD simulations used to define isotherm velocity (*V*) and thermal gradient (*G*) in solidified casting "A".

Table 2. CFD Fluent simulation conditions.

Parameters	Details	Comments
Boundary conditions: - casting-mold boundary - mold– environment - chill - water	 - coupled - air convection - constant temperature	 - no heat resistance
Mesh, cells	- 100 000	
Solver	- transient, pressure based	
Models (designated in article): - method 1 ("flow") - method 2 ("no flow") - method 3 ("adjusted K")	 - coupled Energy, Laminar Flow, Gravity - Energy - Energy	 - buoyancy driven flow - stagnant melt - adjusted K_{aj}
Material properties[29]: - liquidus temperature - solidus temperature - specific heat - density - coefficient of thermal conductivity: - *K* (stagnant melt) - K_{aj} (adjusted *K*)	 -1 395°C -1 370°C - temperature dependent - temperature dependent - temperature dependent - adjusted at T > $T_{dendrite\ coherency}$ [25,30]	 $T_{dendrite\ coherency}$ from [30]
Hunt's model: -criterion -critical equiaxed fraction -controlled isotherms	 $G^{3.4}/V = cst$ 0.5 1 381°C and1 383°C	 [23]

tance between these isotherms in cooling direction. Tracking the position of each isotherm every 5–10 sec of casting solidification was used to determine isotherm velocity (V). After that, a modified Hunt's criterion was calculated as an equivalent of G^n/V, with $n=3.4$.[23)]

In this study, these two macro-parameters (G and V) were defined from a CFD simulated temperature field in the whole solidified casting using a fine mesh. However, their values could deviate from the local thermal gradient and dendrite tip grow velocity.

3. Results

3.1. Model Adjustment

Figure 4 presents comparison of the experimental and simulated cooling curves in the Casting A at two points: near the casting wall and near the casting center in the middle horizontal section. Computational approaches are listed in legend. The overall simulated solidification time was in reasonable agreement with all models. The coupled "flow" model better presents an initial period of removing melt superheat at the casting center while the "adjusted K" model improved the predictions when compared to the "no flow" model.

Details of buoyancy driven flow in the casting "A" (vertical cylinder) during solidification are shown in **Fig. 5**. The peak of the average flow velocity in the casting takes place during first from 15 seconds while the melt flow stopped after 70 seconds (Fig. 5(a)). Vertical velocity (V_z) has a negative value near the casting wall (blue color on map) and a rising stream in the center (Fig. 5(b)) that delivers hot metal to the casting top and deforms the shape of the isotherm during casting solidification (Fig 5(c)).

The solved temperature fields in the casting were used to determine a thermal gradient (G) and an isotherm velocity (V) near 0.5 solid fraction. The thermal gradient decreased during the progress of solidification in the casting (**Fig. 6**(a)).

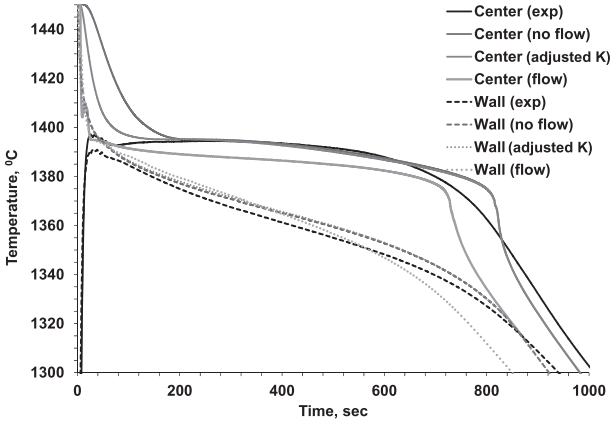

Fig. 4. Experimental and simulated cooling curves in casting "A" (base).

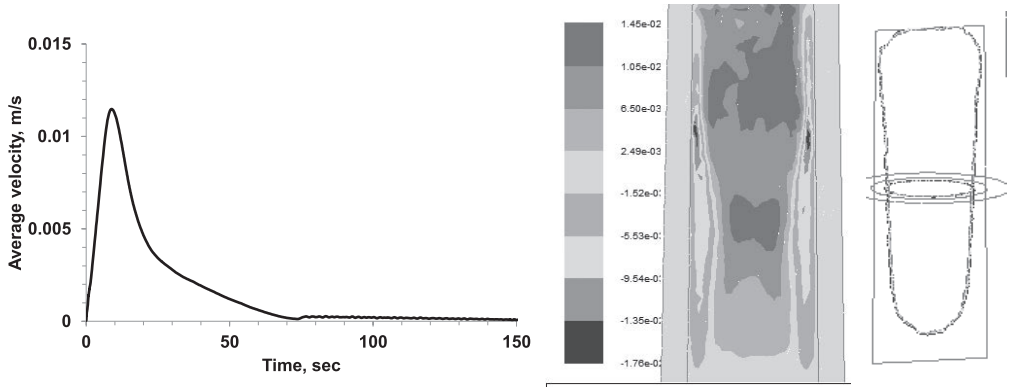

(a) (b)

Fig. 5. Effect of free convection: (a) average melt velocity, (b) map of vertical component of velocity (V_Z) at 20 sec and (c) isotherms (1 381°C and 1 383°C) at 220 sec in vertical section on casting "A".

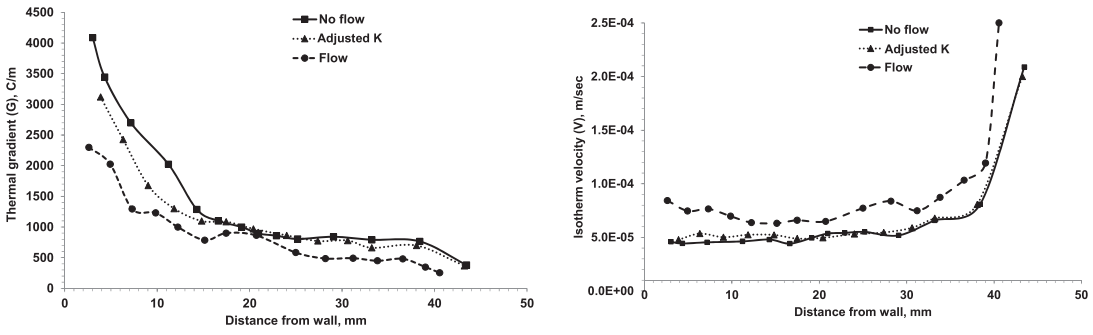

(a) (b)

Fig. 6. Simulated thermal gradient (G) (a) and isotherm velocity (V) (b) in middle horizontal section of casting "A" at 50% of solid fraction using different modelling approaches.

The "flow" model showed a lower thermal gradient than predicted by the "no flow" model because heat was transferred by laminar convection, rather than only by conductivity of still melt. The "adjusted K" model was in reasonable agreement with the "flow" model. However, some differences in the predicted isotherm velocity between the "flow" and "no flow" models were not compensated by applying K_{aj}. Also, partial deformation of the isotherm in a vertical section was not predicted in either model which ignored melt flow.

Simulated thermal gradient (G) and isotherm velocity (V) at 50% solid in the central horizontal section of the casting "A" were used to calculate the modified Hunt's criterion number that is equal to $G^{3.4}/V$. The results for the three modelling approaches are shown in **Fig. 7**(a). The central horizontal macrostructure of the base casting "A" is shown in Fig. 7(b). The macrostructure has a ring of columnar crystals with 40+/−5 mm internal diameter and a restricted central area with large equiaxed crystals. The experimental position of the CET was transferred into the CFD simulated Hunt's criterion graphs (Fig. 7(a)). The critical values of $G^{3.4}/V_{CET}$ for the studied ASS grade produced by the base experimental casting process were obtained for three studied CFD models. In this article, the value of $G^{3.4}/V_{CET}=1\times10^4$ was determined from an "adjusted K" model and the experimentally measured columnar zone thickness (40 mm) was used to predict the position of the CET in the other heavy section castings poured at the same base conditions.

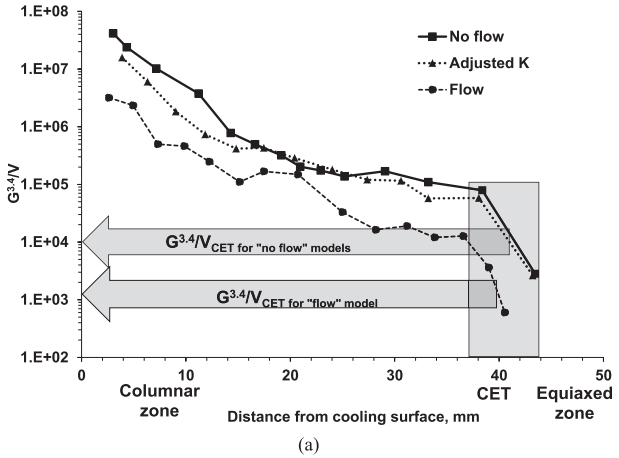

(a)

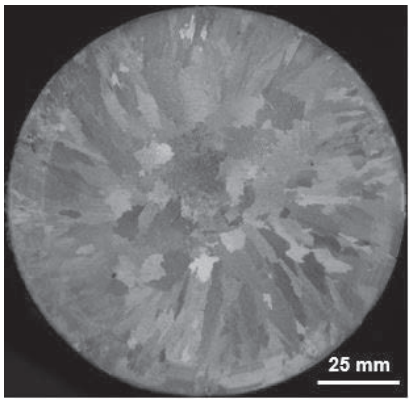

(b)

Fig. 7. Simulated Hunt's criterion graphs for the different CFD macro-models (a) and experimental macrostructure of casting "A" (b). A location of the experimental CET in the casting "A" was used to define the critical $G^{3.4}/V_{CET}$ values for the different CFD models. The "adjusted K" model was used in this article to predict CET in heavy section casting.

3.2. Prediction of CET in Heavy Section ASS Casing

Casting "B" was a heavy section rectangular block made from base ASS using liquid metal processing similar to that used for casting "A". A CFD model with adjusted K was used for solidification simulation of this casting. The simulated values of the modified Hunt's criterion are given in **Fig. 8** for three directions: vertical direction (in the middle vertical section from the casting bottom) and two directions (long and short) along the middle horizontal section. The corresponding position of CET was found using the critical $G^{3.4}/V$ as found for casting "A" for similar base ASS. These predicted values are shown on the corresponding macrostructures of central sections of this casting (Figs. 8(b), 8(c)). The predicted locations of CET in three directions were close to the observed CET in experimental heavy section casting "B".

4. Control of Macrostructure

The two options to control macrostructure and columnar to equiaxed grain ratio in heavy section cylindrical castings were explored and simulated.

4.1 Extensive Columnar Structure

Casting "C" had a similar cylindrical shape as a casting "A" while the mold bottom had a copper water-cooled chill plate and the cylindrical casting wall was formed in an insulating sleeve for directional solidification (from the bottom to the top). **Figure 9**(a) compares experimentally measured and simulated (adjusted K model) cooling curves obtained

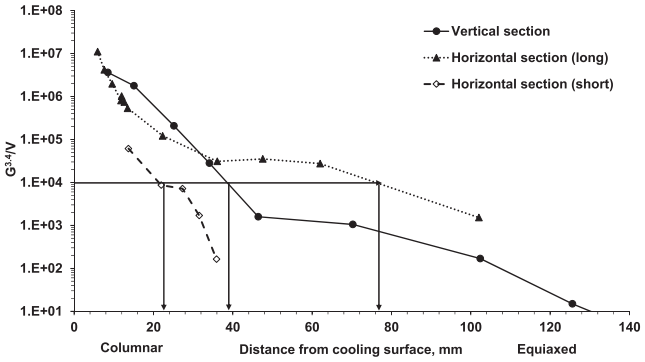

(a)

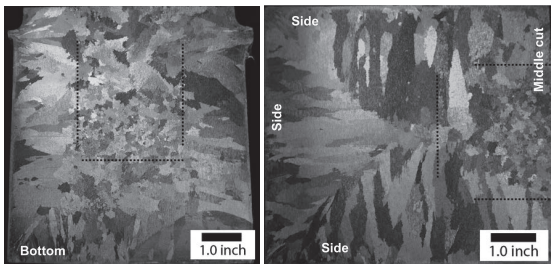

(b) (c)

Fig. 8. Simulated modified Hunt's criterion from the CFD model with adjusted K for three perpendicular directions in the middle sections of casting "B" (a) and the macrostructures of central vertical section (b) and ½ of middle horizontal section (c). Dashed lines - predicted CET.

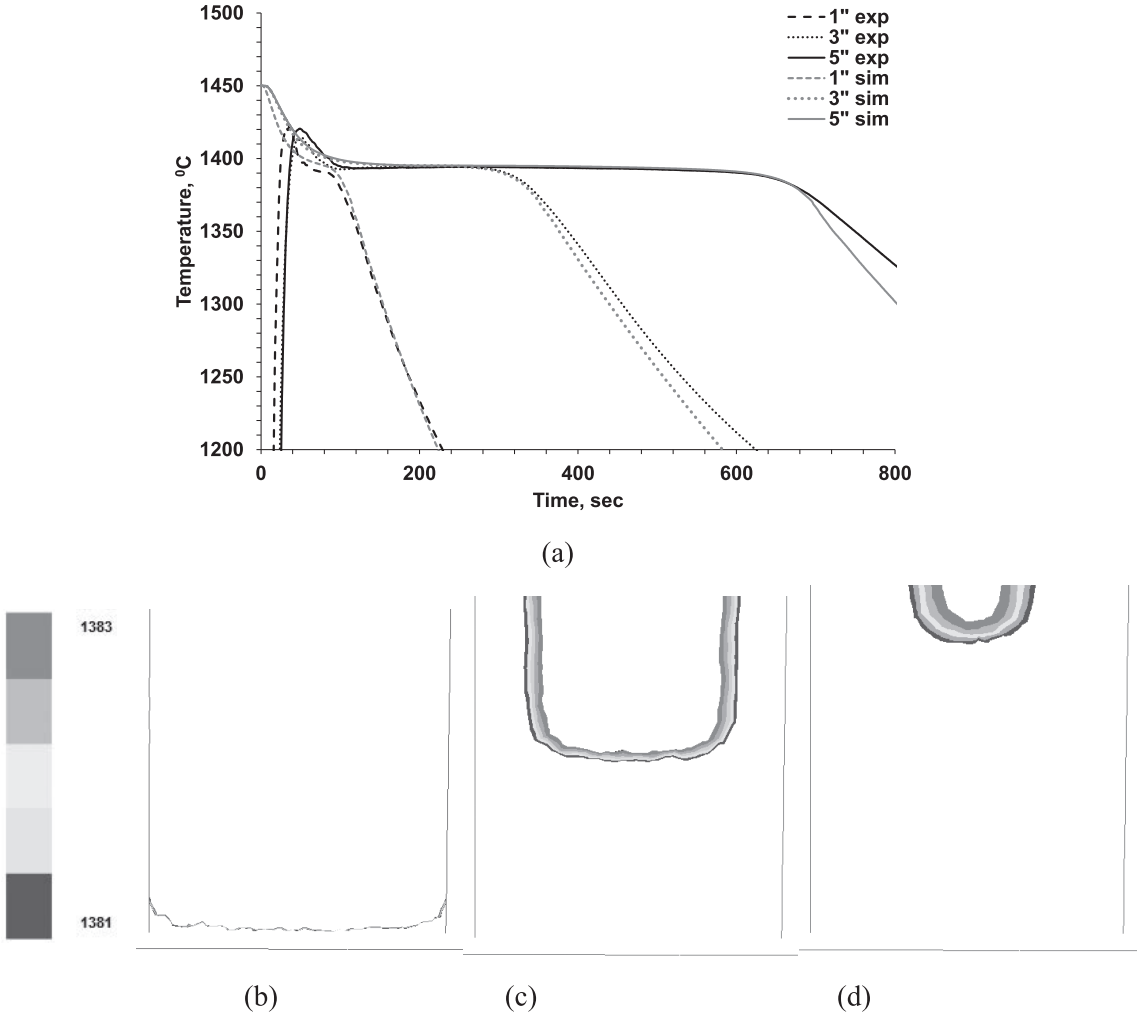

Fig. 9. Comparison of experimental and simulated cooling curves obtained from casting "C" at different thermocouple locations (a), and three isothermal curves in mushy zone of solidified casting at 14 sec (b), 260 sec (c), and 480 sec (d).

from three thermocouples positioned at different distances from the chill bottom: 1" (25 mm), 3" (76 mm), and 5" (127 mm). The solidification sequences indicated well-organized directional solidification from the bottom and the simulated curves were in reasonable agreement to experimental values. Obtained positions of isotherms (1 381°C and 1 383°C) in the mushy zone are shown in Figs. 9(b)–9(d). The solidification front was flat and horizontal near the chill. After that, two solidification zones were formed: one central with a cone shape and approximately 4"–5" (101–127 mm) tall and the other casting volume solidified progressively in a radial direction from the wall.

The values of the modified Hunt's criterion $G^{3.4}/V$ for the directionally solidified casting "C" are shown in **Fig. 10** for the central vertical direction in comparison to the casting "A" and the casting "B". Applying the critical number of the modified Hunt's criterion, an elongated columnar zone from chilled surface up to 100 mm was predicted. The predicted absence of CET in the chilled casting was in agreement with the experimental macrostructure (Figs. 10(b)–10(c)). Only a few equiaxed grains were observed in the horizontal section at 4.5" (114 mm) from the chilled bottom.

4.2. Extensive Equiaxed Structure

To extend the equiaxed grain zone, an effective grain refinement treatment was applied to the casting "A". The developed grain refining technique has been described elsewhere.[2] The resulting structure in the casting "A" after grain refining is shown for both central horizontal (**Fig. 11**(b)) and vertical (Fig. 11(c)) sections. Most of the casting volume had fine equiaxed grains with approximately 0.5" (12 mm) columnar zone. The "base" and the grain "refined" castings "A" solidified at the same cooling conditions, therefore they had the same simulated modified Hunt's criterion curve (Fig. 11(a)). A new critical $G^{3.4}/V$ value for grain refined alloy was obtained by comparison with CET in the grain refined casting "A". The critical value of $G^{3.4}/V$ in the grain refined steel was two orders of magnitude larger than in the base ASS. A grain refined melt has a much larger number of nuclei (N) which increases the critical value of Hunt's number (Eq. (4)).

5. Discussion

This study supports published investigations which conclude that a Hunt macro-model reasonably well predicts CET in different solidification processes: laser welding,[23] continuous casting 16% Cr ferritic stainless steel,[24,25] re-melted ingots from *Ni*-based superalloy,[26] and inoculated aluminum alloys.[27] In this article, the Hunt macro-model

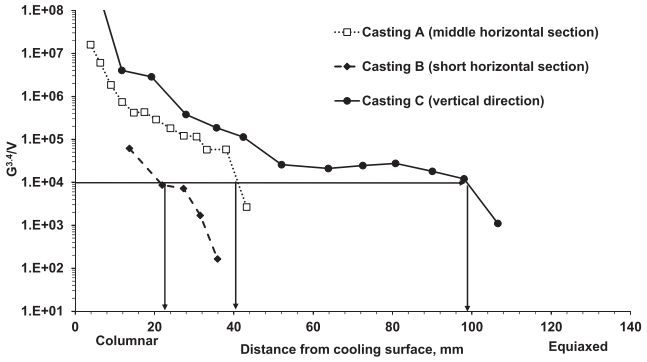

(a)

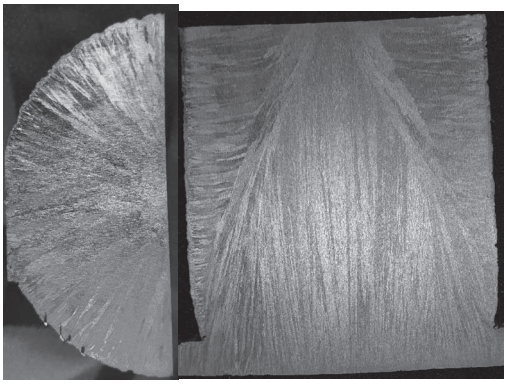

(b) (c)

Fig. 10. The simulated values of the modified Hunt's criterion $G^{3.4}/V$ for directionally solidified casting "C" (adjusted K model) in comparison to castings "A" and "B" (a); macrostructure of casting "C" in the horizontal section at 4.5" (114 mm) from bottom (b), and macrostructure in a central vertical section (c).

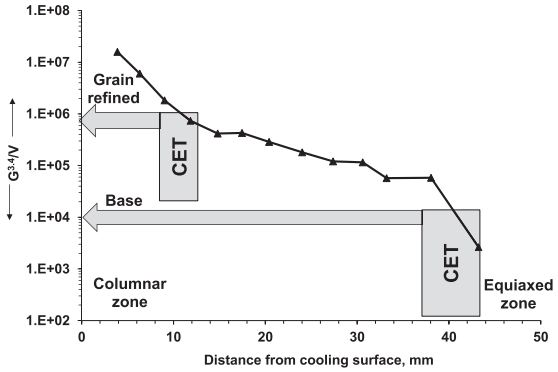

(a)

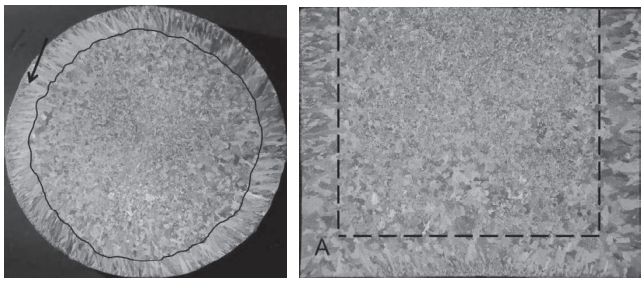

(b) (c)

Fig. 11. Critical values of modified Hunt's criterion for base and grain refined ASS (a) and grain refined macrostructure in central horizontal (b) and vertical (c) sections.

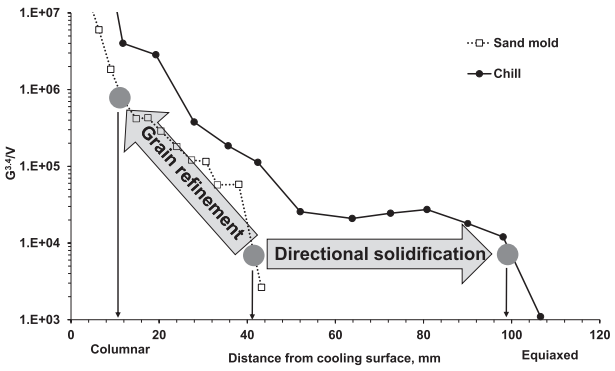

Fig. 12. $G^{3.4}/V$ vs distance from the cooling wall graph illustrates the procedure for calculating the critical value $G^{3.4}/V$ from one experimental casting to another with different metallurgical conditions. This can be applied for prediction of CET.

was used for evaluation of the critical modified Hunt criterion $G^{3.4}/V$ for the ASS castings produced by different metallurgical processing (chilled and grain refined). This critical number was found by superimposing experimentally obtained CET_{exp} on a CFD simulated graph of $G^{3.4}/V$ plotted against distance from the cooling wall (**Fig. 12**, central red dot for cylindrical casting "A").

This method only needs one critical number for Hunt's criterion which was obtained from experimentally observed CET in the casting "A". This number is valid for a particular alloy and processing condition. A prediction of the CET in any other geometry castings or castings subjected to different cooling methods can be made by using the same number. For this, the known critical number needs to be translated on CFD simulating $G^{3.4}/V$ vs distance plot from cooling wall graph for that casting (right dot on Fig. 12 for bottom chilled cylindrical casting "C"). The experimentally observed CET for casting "C" produced with a chill and a heavy section block (casting "B") were in agreement with such predictions.

However, if the same casting is produced from another alloy or by a different metallurgical processing path which affects the dendrite growth or number of nuclei (grain refining, for example), a new experiment will be required to obtain the critical $G^{3.4}/V$ number (left top red dot on Fig. 12). After that, the CET transition could be predicted in a casting made with any shape or cooling condition used for the new processing path.

The coupled Energy and Laminar Flow in Gravity CFD simulations model the effects of melt flow induced by phase density change and solidification shrinkage on an isotherm velocity (V) and the thermal gradient (G) in a mushy zone. These coupled models will provide more detailed three-dimensional geometry of the CET in heavy section castings connected to risers; however, these models are more computationally intensive. For a low pouring superheat, which is typically used for heavy section castings, the "adjusted K" model is recommended for the sake of simplicity.

The described calculation procedure of the critical value of Hunt's criterion has some similarity with simulation of the Niyama criterion ($Ny = G\sqrt{T}$', where T' is cooling rate).[31] The Niyama criterion is defined at 0.1 solid fraction (near liquidus) to predict shrinkage porosity. These two criteria (Hunt and Niyama) cannot deliver the detailed

micro-scale analysis, such as particular grain sizes (for Hunt criterion) or shape of shrinkage pores (for Niyama criterion). However, Niyama analysis is very useful when designing gating systems and risers for sound castings. Similarly, Hunt criterion mapping could be also useful to design processes for a preferred type of macrostructure in austenitic and ferritic stainless steel, which have limited capabilities to change the macrostructure in solid state because of the lack of polymorphous transformations.

6. Conclusions

Several castings from ASS were produced to verify the effects of casting geometry, chilling, and grain refinement on the CET. A simulated transient thermal field for several solidified castings was used to determine an isotherm velocity (V) and a thermal gradient (G) in the melt at 0.5 solid fraction. The critical value of the modified Hunt parameter G^n/V was determined from the macrostructure of the cylindrical casting. Using this value, the location of the CET was predicted in a heavy rectangular casting and this prediction was in agreement with the experimentally observed macrostructure. Two methods of controlling casting macrostructure were verified experimentally by promoting an extensive columnar zone in a chilled mold and by producing a fine equiaxed grain structure using melt grain refinement. The predicted CET was in agreement with the experimental CET. It was found that the Hunt criterion mapping of CFD simulated temperature fields is a useful tool when designing processes for a preferred change macrostructure.

Acknowledgements

This study is supported by Kent Peaslee Steel Manufacturing Research Center and the authors gratefully thank to the members of the industrial advisers committee of this project for material supply, suggestions in mold design, and regular results discussion. The authors thank Dr. V. Richards for helpful discussion and Dr. D. Robertson for comments that greatly improved the manuscript.

REFERENCES

1) S. M. Seo, I. S. Kim, C. Y. Jo and K. Ogi: *Mater. Sci. Eng. A*, **25** (2007), 713.
2) S. N. Lekakh, J. Ge, V. Richards, R. O'Malley and J. R. TerBush: *Metall. Mater. Trans. B*, **48** (2017), Issue1, 406, DOI: 10.1007/s11663-016-0832-5.
3) X. Wu, Y. Yang, J. Zhang, G. Jia and Z. Hu: *J. Mater. Eng. Perform*., **8** (1999), 525.
4) J. Z. Lu: *Acta Mater*., **58** (2010), 5354.
5) B. Abbasi-Khazaei: *J. Mater. Sci. Technol*., **10** (2012), 946.
6) O. Grong: *ISIJ Int*., **46** (2006), 824.
7) R. Tuttle: *Int. J. Metalcast.*, **6** (2012), issue 2, 51.
8) J. S. Park and J. H. Park: *Steel Res. Int*., **85** (2014), 1303.
9) J. D. Hunt: *Mater. Sci. Eng*., **65** (1984), 75.
10) W. Mirihanage, H. Dai, H. Dong and D. Browne: *Adv. Eng. Mater*., **15** (2013), 216.
11) S. McFadden and D. Browne: *Appl. Math. Model*., **22** (2009), 1397.
12) C. Wang and C. Beckermann: *Metall. Mater. Trans. A*, **25A** (1994), 1081.
13) A. Badillo and C. Beckermann: *Acta Mater*., **54** (2006), 2015.
14) J. Banaszek, S. McFadden, D. Browne and G. Zimmermann: *Metall. Mater. Trans. A*, **38A** (2007), 1476.
15) D. Carvalho, A. Moreira, D. Moutinho, J. Filho, O. Rocha and J. Spinelli: *Mater. Res*., **17** (2014), 498.
16) M. Rappaz and C. A. Gandin: *Acta Metall. Mater*., **41** (1993), 345.
17) C. A. Gandin and M. Rappaz: *Acta Mater*., **45** (1997), 2187.
18) FESI Group: ProCast, FESI Group, France, http://www. Esi-group.com, (accessed 02-01-2016).
19) J. Roucka, V. Kosour, M. Kovac, V. Krutis and K. Hrbacek: *IOP Conf. Series: Mater. Sci. Eng*., **33** (2012), DOI: 10.1088/1757-899X/33/1/012085.
20) A. Burbelco, J. Falkus, W. Kapturkiewicz, K. Solek, P. Drozdz and M. Wrobel: *Arch. Metall. Mater*., **57** (2012), 379.
21) H. Dai, J. Debelin and M. Newell: Superalloys 2008, TMS, Warrendale, PA, (2008), 367.
22) P. Lan, H. Tang and J. Ahang: *Metall. Mater. Trans. A*, **47** (2016), 2964.
23) W. Kurz, C. Bezencon and M. Gaumann: *Sci. Technol. Adv. Mater*., **2** (2001), 185.
24) J. C. Kim, J. J. Kim, J. Y. J. Y. Choi, J. H. Choi and S. K. Kim: La Metallurgia Italiana, September 2009, AIM, Milano, (2009), 43.
25) H. Shibata, S. Itoyama, Y. Kishimoto, S. Takeuchi and H. Sekiguchi: *ISIJ Int.*, **46** (2006), 921.
26) A. Mitchell: *Inter. J. Cast. Met. Res*., **22** (2009), 216.
27) D. Pineda and M. Martorano: *Acta Mater*., **61** (2013), 1785.
28) ANSYS: Fluent, USA, http://www. ansys.com, (accessed 02-10-2015).
29) Sente Software Ltd.: JMatPro,UK, http://www.sentesoftware.co.uk, (accessed 08-20-2016).
30) S. Lekakh and V. Richards: AFS Proc., Paper 11-042, American Foundry Society, Schaumburg, IL, (2011), 1.
31) K. Carlson, S. Ou, R. Hardin and C. Beckermann: *Metall. Mater. Trans. B*, **33B** (2002), 731.